An Aqueous, Electrode-Decoupled Redox-Flow Battery for Long Duration Energy Storage

Shrihari Sankarasubramanian
Washington University in St. Louis https://orcid.org/0000-0002-0338-4009
Yunzhu Zhang
Washington University in St. Louis
Cheng He
Washington University in St. Louis
Thomas Gregory
Borealis Technology Solutions
Vijay Ramani (ramani@wustl.edu)
Washington University in St. Louis https://orcid.org/0000-0002-6132-8144

Physical Sciences - Article

Keywords: redox-flow battery, anion exchange membrane, grid-scale energy storage, long duration energy storage (LDES)

Posted Date: January 27th, 2021

DOI: https://doi.org/10.21203/rs.3.rs-150474/v1

Abstract

Redox-flow batteries (RFBs) enable large-scale energy storage at low cost due to the independent scaling of device power and energy, thereby unlocking energy arbitrage opportunities and providing a pathway to grid stability and resiliency. Herein we demonstrate an “electrode-decoupled” redox-flow battery (ED-RFB) with titanium and cerium elemental actives that has a clear pathway to achieve a levelized cost of storage (LCOS) of *ca* $0.025/kWh-cycle. A key enabling technology is our highly perm-selective modified poly(ether ketone)-based anion exchange membrane (AEM) that ensures long term separation of Ti and Ce species and enables capacity-fade-free cycling over 1300 hours of operation. Further, our Ti-Ce ED-RFB exhibits negligible capacity fade when the actives are charged to 90% state of charge (SOC), stored for close to 100-hours and then discharged, rendering it viable for long duration (load-following) grid-scale energy storage applications. Herein we introduce the Ti-Ce ED-RFB as a novel, low-cost long duration energy storage (LDES) system.

Introduction

The sustained fall in the cost of solar photovoltaic and wind energy has led to a market-driven increase in their deployment in the electricity grid.[1–4] Ensuring reliability and resiliency of the increasingly renewables-powered grid will require the deployment of suitable energy storage technologies.[5–8] Deployment of energy storage resources at scale will in turn drive innovation, expand economies of scale, reduce costs and setup a virtuous cycle of increasing decarbonization.[4,9–11] Typical batteries (e.g., Li-ion batteries) seldom maintain discharge at peak power for durations sufficient to regulate power output from intermittent sources.[12] On the other hand, redox-flow batteries (RFBs) are excellent candidates for grid-storage applications[13] wherein the electroactive materials are externally stored and pumped into the electrochemical stack as required, decoupling the energy and power obtainable from a given unit. The energy is a function of the amount of externally stored electroactive material while the power is a function of the stack size, allowing for independent scaling of device energy and power, in turn ensuring sub-linear scaling of the system cost with scale.[14,15]

Thaler and co-workers at NASA demonstrated the first RFB in the 1970s[16] based on the Fe-Cr[17–19] chemistry. Despite years of effort, this relatively cost-effective system suffers parasitic side-reactions whose mitigation requires complex system-level changes.[19–21] This has led to the failure of multiple commercial ventures deploying this technology.[22] In the 1980s the all-V RFB[23,24] was developed by Skyllas-Kazacos and co-workers and this chemistry is the farthest along in terms of commercial development. Despite the operational advantages of using the same elemental active on the cathode and anode sides, vanadium is cost-prohibitive, geographically limited in availability (and hence geopolitically constrained) and is not likely to meet system-level cost targets.[5,15] Numerous other elemental active combinations have been demonstrated in RFBs with some examples being the Zn-Ce[25–27], all-Fe[28,29], Ce-Pb[30], V-Ce[31–33], Zn-V[34], Cr-Zn[35] chemistries. The challenges in each case have been a combination of high cost, parasitic side reactions (e.g., H_2 evolution), durability, difficulties with phase-change at the

electrode (plating/dissolution), and reactant-cross-over-driven capacity-fade. More recently, aqueous RFBs with organic actives[36–39] and non-aqueous RFBs[40–43] have been investigated. Aqueous RFBs featuring organic active species suffer from side-reactions involving the very same electroactive centers in these molecules. A prominent example is the dimerization of methyl viologen based actives.[44–46] Further, these systems claim cost-effectiveness once the production of the proposed actives are scaled up.[14,15,47] Currently no economic or market incentives exist for investments in the production of these organic actives, which in turn has to be followed by additional capital investments to manufacture the RFBs at scale. Organic RFBs suffer from significantly higher costs due to the nature of the solvents and actives used.[14,15] Thus, no commercial RFB systems employing organic actives in aqueous media or organic electrolyte solvents currently exist.

We posit that viable RFB alternatives to mass-produced energy storage systems such as Li-ion batteries (that linearly scale in terms of cost due to coupling of energy and power) should utilize electrolyte precursors that are already produced at scale and require minimal processing. Further, any RFB system should meet the overall DOE / ARPA-E cost targets that have been documented to have any chance at a viable pathway to commercialization.[5,48,49] In this paper, we: **a)** identify the characteristics of such an ideal RFB system, **b)** identify Ti and Ce as abundantly available electroactive species satisfying these criteria, **c)** elucidate their electrochemistry, **d)** develop a Ti-Ce electrode-decoupled RFB (ED-RFB) employing our unique and highly perm-selective anion exchange membrane (AEM) separator that permits the use of dis-similar actives at either electrode without irreversible capacity-fade, **e)** test the ED-RFB over a long time frame (1300 hours) employing long-duration (24-hr) cycles that mimic real world usage, and **f)** show through detailed techno-economic analyses that our ED-RFB system can comfortably attain a levelized cost of storage (LCOS) of <$0.05/kWh-cycle when deployed at scale, thereby being cheaper then established DOE targets for grid-storage applications.

The development and utilization of our highly perm-selective AEM separator is particularly noteworthy as it permits electrode-decoupled operation with minimal to no intermixing of the cations in the catholyte and the anolyte, thereby doubling the usable capacity of the cell.[31,50,51] The electrode-decoupled operation greatly expanded the chemical design space available for the choice of actives, resulting in the development of the aqueous Ti-Ce ED-RFB.

Results And Discussions

The desired design characteristics of an ideal redox-flow battery (enumerated below and expanded upon in Supporting Materials section S1) were determined after taking into consideration the problems and challenges identified in existing systems[13,52,53] and with the aim of keeping the overall cost under $100/kWh[5,15,49]:

1. High coulombic efficiency: Minimal parasitic side-reactions or gas-evolution (H_2 or O_2) reactions during operation.

2. Nominal operating cell voltage ≥ 1V and low equivalent weight of active materials to reduce cost/kWh.
3. No reactions involving phase change at either electrode: Multiple (soluble) oxidation states needed for the electroactive species.
4. Low cost: Aqueous electrolytes combined with low-cost and currently mass-produced electro-actives with good solubility.
5. Benign (non-toxic, no side reactions).

By examining various electroactive species soluble in aqueous electrolytes (Supplementary Materials **Fig. S1**), several possible combinations that could constitute cells with ≥ 1V were identified. Unfortunately, the cells with the highest nominal voltages, namely the Zn-Ce and Zn-Br systems do not meet the phase change criterion, with Zn dendrite mitigation being a perennial problem.[25,54] The Fe-Cr system, with a nominal voltage of 1.19V suffers from irreversible side reactions and H_2 evolution at the Cr electrode.[19] The methyl viologen and ferrocenium based actives (from the work of Aziz and co-workers[37] and representative of the class of similar organic actives) do form ≥ 1V cells in combination with elemental actives at the other electrode but their long-term stability and cost-effective production at scale has not been demonstrated. And while the all-V system is outstanding in many respects, the cost of vanadium is such that the cost of actives alone would exceed the DOE cost target for the RFB system.[5,48,49]

The elemental actives were next examined in the context of their abundance in the Earth's crust as well as their broad availability, and hence their potential for meeting large-scale deployment on the worldwide electric grid. Figure 1**(a)** depicts the abundances of some of the electroactive elements that satisfy one or more of the criteria outlined above.[55] Ti was found to be 20x as abundant as V and hence would be an excellent replacement for V-based RFBs. Given that the E^0 of the TiO^{2+}/Ti^{3+} couple is 0.19V vs. SHE, it has to be paired with the Ce^{3+}/Ce^{4+} couple to produce a cell with a nominal voltage ≥ 1V. Despite being a so called "rare earth" element, Ce is as abundant as Pb (found in lead-acid batteries used in every internal combustion gasoline vehicle on the road today) and is almost 2x as abundant as Co, which is critical to Li-ion batteries. The existing proven reserves depicted in Fig. 1**(b)** can enable Ti-Ce RFBs to store over 300 times the entire world electricity production (25,000 TWh/year) (see production data in Fig. 2) even based on the limiting species, Ce. Figure 1**(c)** and **(d)** identify the countries with the top 5 proven reserves of Ti and Ce. The existence of reserves does not necessarily indicate the level of development or exploitation of those reserves, but the wide geographical spread of these reserves could make Ti and Ce supply immune to geopolitical shifts. Thus, the combination of Ti and Ce satisfied all of our technical criteria and also offered several economic and geopolitical advantages and hence was chosen for further study.

A schematic for our Ti-Ce ED-RFB is depicted in Fig. 2**(a)**. The highly permselective AEM ensures that ion conduction across the separator occurs primarily by the transport of anions as depicted in Fig. 2**(b)**. The corresponding electrode half-cell reactions are as follows –

Ti^{4+} (as TiO^{2+}) + $e^- \leftrightarrow Ti^{3+}$ (E^0 = 0.19V vs. SHE) - Negative Electrode

$Ce^{4+} + e^- \leftrightarrow Ce^{3+}$ (E^0 = 1.61V vs. SHE) – Positive Electrode

The Ti and Ce electrolytes were formulated with a variety of supporting electrolytes that are stable across the voltage window of these redox couples (Supplementary Materials **Section S2**). Only acidic supporting electrolytes were examined, as the soluble oxidation states desired as per the half reactions presented above occur only at low pH (see Pourbaix diagrams in Supplementary Materials **Fig. S2**). Given the highly oxidizing nature of Ce^{4+}, side-reactions with the supporting electrolyte is a concern (Supplementary Materials **Fig. S3**). The down-selection of suitable supporting electrolytes (from amongst HCl, H_2SO_4, HNO_3 and CH_3SO_3H) is detailed in Supplementary Materials **Section S2**. Both H_2SO_4- and CH_3SO_3H-supported electrolyte formulations were identified as the only stable combinations; the side-reactions encountered with HCl and HNO_3 are discussed in Supplementary Materials **Section S2**. The choice of supporting electrolytes was found to significantly affect the E^0 value of the Ce^{3+}/Ce^{4+} redox couple, with a 120mV difference between H_2SO_4 and CH_3SO_3H supported electrolytes in line with earlier reports.[56] Ce^{3+} and Ce^{4+} exhibit diametrically opposite solubility behavior with increasing acid concentration with Ce^{3+} solubility decreasing while Ce^{4+} solubility increases (Supplementary Materials **Fig. S4**).[57] The maximum achievable solubility where both species stay in solution is 0.5M in H_2SO_4 and 0.9M in CH_3SO_3H and hence these concentrations were used at the positive electrode.

Unlike the constraints on the Ce electrolyte, $TiOSO_4$ was found to be highly soluble in H_2SO_4 and solutions of up to 10M have been prepared and characterized as shown in Supplementary Materials **Fig. S6.** Ti is much less readily soluble in CH_3SO_3H with concentrations of 6M resulting in precipitation of the Ti salt as seen in **Fig. S6.** Nevertheless, Ce is by far the limiting species, and achieving sufficient Ti concentration at the negative electrolyte is not an issue.

Cyclic voltammograms (CVs) with Ti and Ce electrolytes indicated that a mixed supporting electrolyte consisting of H_2SO_4 and CH_3SO_3H is ideal in terms of reversibility (inferred from the CV peak separation ΔE_p) and energy efficiency (directly proportional to the voltage efficiency, which is a function of reversibility) of the system (see Supplementary Materials **Fig. S7**). However, issues with variable and inversely correlated solubility of the Ce^{3+} and Ce^{4+} ion led us to avoid using these mixed systems pending further fundamental studies.[57] The CVs depicting the Ce and Ti half-cell reactions with H_2SO_4 as the supporting electrolyte are depicted in Fig. 2**(d)**. The Ce redox peaks show a separation of 0.76V while the Ti peaks are separated by 1.53V. Similarly, CVs depicting the Ce and Ti half-cell reactions with CH_3SO_3H as the supporting electrolyte are depicted in Fig. 2**(e)**. The Ce redox peaks show a separation of 0.67V while the Ti peaks are separated by 1V. Given the > 59mV peak separation, both half-reactions are not reversible.[58] This resultant differences between the average charge and discharge voltages for the Ti-Ce ED-RFB can be mitigated by suitable surface treatment of the RFB electrodes.[59] This will in turn influence the voltage efficiency and hence energy efficiency of the RFB. Despite the differences in ΔE_p, the differences in formal potentials $E_{form} = (E_{cathodic} + E_{anodic})/2)$ ensures that the theoretical open circuit potential (OCP) for the Ti-Ce ED-RFB is *ca* 1.36V with the CH_3SO_3H supported electrolytes exhibiting a

slightly higher OCP (~ 20mV higher) due to the observed shift in $E_{1/2}$ of the Ce electrolyte when used with CH_3SO_3H. Ce^{4+} was verified to not cause any unwanted oxidative reactions in both systems. Supplementary Materials **Section S3.2** details the calculation of the diffusion coefficients of Ce and Ti redox species in H_2SO_4 and CH_3SO_3H supporting electrolytes (values tabulated in **Table S1**) using the Nicholson-Shain method.[60] Diffusion coefficients were higher for Ce species as compared to Ti species, and higher diffusion coefficients in CH_3SO_3H-supported electrolytes suggested reduced complexation with both Ti and Ce following Pearson's hard-soft acid-base theory.[61,62] The first electron transfer rate constants (k_0) for both the Ce and Ti redox couples were also calculated from the CVs using the method of Kochi and Klingler as detailed in Supplementary Materials **Section S3.3**.[63] Reduced complexation in CH_3SO_3H-supported electrolytes led to higher k_0 values in these electrolytes. The k_0 values for the Ti redox couple in both supporting electrolytes were 3-orders of magnitude lower than for the Ce redox couple, indicating that negative (Ti) electrode is rate limiting. The H_2SO_4- and CH_3SO_3H-supported electrolyte formulations were tested further in RFBs.

Having identified and characterized suitable Ti and Ce electrolytes, the key requirement to realize an ED-RFB is a highly permselective AEM. We selected a quaternized cardo-poly(ether ketone) (QPEK-C)-based AEM functionalized with trimethylamine (TMA) (depicted in Fig. 2**(c)**). We have previously reported this separator[31] and composites thereof incorporating metal oxide nanoparticles[50] to improve permselectivity. We have significantly enhanced the permselectivity reported in our previous work by judiciously incorporating various metal oxide nanoparticles (details in Supplementary Materials **Section S4** and AEM characteristics in **Table S3**). The resultant permselectivity improvement is summarized in Fig. 3 in terms of the permeability coefficient, a time-independent measure of permeation of a given species across a separator.[47,64] QPEK-C-TMA AEMs incorporating Al_2O_3 nanoparticles exhibited the lowest permeability coefficient, equivalent to < 0.4% undesired cross-over of cations over 1000 hours, which compares very favorably in terms of capacity-fade with extant state-of-the-art technologies.[47]

Ti-Ce ED-RFBs incorporating pristine QPEK-C-TMA and its metal oxide nanoparticle enhanced variants were tested (details in Supplementary Materials **Section S6**) and the performance of the ED-RFB with H_2SO_4 –supported Ti-Ce electrolytes separated by a Al_2O_3 enhanced QPEK-C-TMA separator is depicted in Fig. 4. The cell was cycled diurnally (i.e., 12-hour charge- 12-hour discharge) for 1300 hours (about 8 weeks) to mimic the load leveling use case on the electric grid. Despite minimal cycle to cycle variations in capacity (Fig. 4 **(a)**), the normalized capacity never fell below 90%. Near 100% capacity retention was observed, indicating that the highly perm-selective separator was indeed mitigating a major route for capacity fade, namely active species cross-over. The area-specific resistance (ASR) of the separator remained unchanged within experimental error over the duration of the run, confirming *ex-situ* observations via ^{13}C-^{1}H 2D NMR and attached proton test (APT) (detailed in Supplementary Materials **Section S5**) confirming that there was no chemical degradation of the QPEK-C-TMA separator in low pH electrolytes (unlike at high pH, wherein AEM degradation is well documented).[65,66] Since chemical degradation affects separator conductivity and the separator is the largest resistive source in the device,

this exceptional separator stability confirms its suitability for long-term operation. The coulombic, voltage and energy efficiencies of the ED-RFB are depicted in Fig. 4 **(b)** (calculations detailed in the Supplementary Materials **Section S6** and elsewhere[67]). As expected from the CVs, the irreversible nature of the Ti and Ce redox couples necessitates the application of higher overpotentials to drive the redox reactions. This directly translates into poorer voltage efficiency. Given that the energy efficiency is a product of the coulombic and voltage efficiencies, the energy efficiency is, on average, *ca* 70%. The observation that changing the supporting electrolyte significantly changes the redox potentials for both half-reactions of interest suggests that the use of electrolyte additives or alternate stable supporting electrolytes provide viable pathways to further increase the voltage efficiency of the Ti-Ce ED-RFB, as does electrode-modification to lower redox-reaction overpotentials. Overall, the highly energy efficient diurnal energy storage performance of Ti-Ce ED-RFB makes it an excellent candidate for grid deployment provided economic pathways exist to achieve the DOE target LCOS of <$0.05/kWh-cycle.

A second grid-scale deployment use case examined was that of long duration energy storage (LDES). Since the RFB places the energy storage media outside the cell itself, the amount of energy that can be stored is limited only by tank size. Thus, the potential exists to scale RFBs to enable multi-day or even multi-week (i.e., extended-duration) energy storage. The key to this use case is the minimization of capacity fade during storage (i.e., self-discharge). The self-discharge performance of the Ti-Ce ED-RFB was examined by cycling it for 100 hours followed by charging it to a 90% state of charge (SOC), withdrawing the charged electrolytes, and storing them in their tanks. After 96 hours of storage, the electrolytes were reintroduced into the RFB and discharged, and the discharge capacity was measured. The polarization performance of the RFB before and after storage at 90% SOC is depicted in Fig. 5**(a)**. The OCP before and after storage was unchanged within experimental error, indicating minimal self-discharge during storage. The polarization curve was also essentially unchanged, as were the activation and ohmic polarization. The near-quantitative absence of self-discharge was confirmed by discharging the cell from 90% SOC (Fig. 5**(b)**). The coulombic efficiency was close to 100% for both this “charge-store-discharge” cycle and for the previous conventional charge-discharge cycle (Supplementary Materials **section S6**). Thus, the Ti-Ce ED-RFB was found to be suitable for both diurnal and for LDES in scenarios mimicking normal grid operations.

The next key consideration in the analysis of the commercial viability of the Ti-Ce ED-RFB is the economics of the system. A comprehensive cost model considering the manufacturing of the AEM separators at various production scales, incorporating ED-RFB component and system-level costs and examining the LCOS is various operational scenarios is presented in Supplementary Materials **Section S7**. The DOE defined component cost target level is <$10/kWh for the separator.[48] Incorporating this separator, the DOE defined system level cost target is <$100/kWh.[5] The separator cost was obtained by developing heuristic process models for its production at 1000 metric tons per annum (MTA) scale with industry appropriate cost scaling factors. The inevitable uncertainty in raw material, utilities, staffing and other operational costs were accounted for by cost sensitivity analysis that let us set bounds for the component and system level costs. The QPEK-C-TMA AEMs were found to cost as little as

$2.5/kW_{eqivalent}$. There was minimal cost impact upon changing the cation in the AEM, with a 100x cation-precursor cost increase resulting in only a 5.5% separator cost increase. Enhancing the permselectivity by incorporating metal oxide nanoparticles into QPEK-C-TMA also had an inconsequential impact on the separator cost as the metal oxide cost and added processing cost was found to be 0.13% of the total separator cost.

The component costs were incorporated into a system cost model with RFBs at the 1MW/4MWh (distributed power system) and 2GW/10GWh (utility integrated system) scales. This analysis considered both the H_2SO_4 and CH_3SO_3H electrolytes and examined the impact of the electrolyte cost on the system cost while accounting for differences in energy density. Interestingly, while the CH_3SO_3H electrolytes cost ~ 4x the H_2SO_4 electrolytes, the near doubling of the energy density meant that the system level cost differential between the H_2SO_4 and CH_3SO_3H based systems was only a factor of 2. Overall, the Ti-Ce ED-RFB was found to cost $90/kWh in the H_2SO_4 configuration, coming in lower than the DOE cost target.[48]

The LCOS was calculated incorporating the system level costs as depicted in **Fig. S22**. The LCOS was calculated for the unoptimized system with performance metrics matching those in the lab. Following this conservative baseline, several scenarios for operational optimization at scale and cost reduction are presented in Fig. 6. Most interestingly, it was found that relatively incremental improvements in the Ti-Ce ED-RFB such as operating at 200 $mA.cm^{-2}$ current density, designs incorporating air cooling of the stack, and changing storage-tank material (and hence cost) significantly impacted the system-level cost. Similar robust pathways to reduce the LCOS were also found to exist (4 scenarios are presented in the Supplementary Materials) with plausible scenarios exceeding the DOE LCOS target of $0.05/kWh-cycle. Thus, we posit that in addition to demonstrated technical viability, the Ti-Ce ED-RFB is an economically viable candidate for grid scale diurnal load leveling and long duration storage applications.

Materials And Methods

Extended materials and methods are available in the Supplementary Materials**.**

Synthesis of the anion exchange membrane (AEM) separator

The separator used herein has been previously reported by us in Yun *et. al.*[51] and the synthesis procedure is unchanged. 10 g of QPEK-C (Xuzhou Vat Chemical Company, China) was dissolved completely in 500 ml 1,1,2,2-tetrachloroethane (98.5%, Acros Organics). 6 g of paraformaldehyde (96%, Acros), 25 ml of Chlorotrimethylsilane (98% Acros), and 0.47 ml of tin tetrachloride (>99%, Sigma Aldrich) were added to a well-stirred solution. The mixture was heated, and the reaction carried out at 80 °C for a week with reflux. The reaction scheme is presented in **Fig. S12**. The reaction solution was precipitated in methanol (3~4 times the volume of the reaction mixture). The white precipitate was filtered and purified by re-dissolving in dimethylformamide (DMF, 99.8%, Acros Organics) followed by re-precipitation in methanol. The purification process was carried out 2~3 times. The precipitate was dried at 40 °C over 12 hours and stored for further use. The white solid CPEK was obtained with a degree of chloromethylation

(chloromethyl groups per polymer repeating unit) of 0.8-0.9. The NMR spectra is shown in **Fig. S13**. 0.5 g of QPEK-C was dissolved completely in 9 ml of DMF followed by the addition of 0.7 ml of trimethylamine (TMA) to the mixture. The solution was stirred and allowed to react at 30 °C for 2 days. The membrane was obtained by casting the reaction mixture onto a 3" x 3" flat glass plate in an oven at 70 °C, heated overnight on a leveled surface. The thickness of the obtained membranes was approximately 40 µm. The measurement methodology for the membrane ionic conductivity and ion exchange capacity is detailed in Supplementary Materials **Section S5**.

Synthesis and characterization of ED-RFB electrolytes

The electrolytes used in this study consisted of two formulations, based on H_2SO_4 and CH_3SO_3H supporting electrolytes, respectively. The composition of the H_2SO_4-supported electrolytes was 0.5M $TiSO_4$ in 4M H_2SO_4 and 0.5M $Ce_2(SO_4)_3$ in 3M H_2SO_4. The composition of the CH_3SO_3H-supported electrolytes was 0.9M $TiSO_4$ in 5.8M CH_3SO_3H and 0.9M $Ce(CH_3SO_3)_3$ in 4M CH_3SO_3H. $TiSO_4$ (97%, Sigma-Aldrich) readily dissolved in water and H_2SO_4 (95-98%, Sigma-Aldrich) or CH_3SO_3H (99%, Acros Organics) to yield the desired electrolyte. The $Ce_2(SO_4)_3$ was made by reacting $Ce_2(CO_3)_3$ (99%, Treibacher Industrie A.G.) with H_2SO_4 as follows –

$$Ce_2(CO_3)_3 + 3H_2SO_4 \rightarrow Ce_2(SO_4)_3 + 3CO_2 + 3H_2O$$

The $Ce(CH_3SO_3)_3$ was made by the reaction between CH_3SO_3H and $Ce_2(CO_3)_3$ [56,68]-

$$Ce_2(CO_3)_3 + 6CH_3SO_3H \rightarrow 2Ce(CH_3SO_3)_3 + 3CO_2 + 3H_2O$$

The $Ce_2(CO_3)_3$ was suspended in DI water and the desired acid was added dropwise with constant stirring. Due to the sensitivity[57] of $Ce_2(SO_4)_3$ and $Ce(CH_3SO_3)_3$ solubility to the acid concentration, the reaction mixture was diluted periodically with DI water to prevent precipitation of the cerium salt. Electrochemical characterization using cyclic voltammetry was carried out in a small-volume electrochemical cell (Pine Instruments, RRPG223) with a 3mm diameter glassy carbon (GC) disc working electrode, a Pt mesh counter electrode and an Ag/AgCl reference electrode. The electrochemical measurements were performed using a Solartron multichannel potentiostat.

Redox-flow battery (RFB) tests

The redox-flow battery testing was carried out using a Scribner Inc. 857 RFB test stand using a $25cm^2$ plate-and-frame configuration cell. The carbon felt electrodes (SigraCELL GFA6, SGL carbon) were activated by heating in air in a muffle furnace at 400°C, immersing in *aqua regia* (1:3 mole ratio of HNO_3:HCl) at 60°C for 4 hours followed by thorough DI water wash and drying in an oven. All tests were carried out using interdigitated flow fields at a flow rate of 100 $mL.min^{-1}$ and at 25°C. The polarization measurements were carried out by initially charging the ED-RFB to the voltage corresponding to the desired state of charge (SOC) and increasing the current stepwise with a 30s hold after each step

increase to allow for equilibration. The initial SOC was maintained by discharging (or charging) the cell for 30s after each 30s hold. The charge-discharge cycling was carried out galvanostatically at a minimum current density of 100 $mA.cm^{-2}$ followed by a potentiostatic hold at the cutoff voltage until the current density trickled down to 4 $mA.cm^{-2}$. The H_2SO_4-based ED-RFBs were charged and discharged between 2V and 0.3V while the cutoffs for the CH_3SO_3H based cells were 1.85V -0.3V. The efficiency calculations for the RFB are detailed in the Supplementary Materials **Section S6**.

Cation cross-over measurements

The cation cross-over was determined by UV-vis spectroscopy. The Ti side of the ED-RFB was drained upon completion of the ED-RFB test and the concentration of Ce^{3+} ions was determined. All RFB tests were completed in such a manner that the final cell state of charge (SOC) was 0% (i.e., complete discharge) so as to have only Ce^{3+} ions in the system. The collected electrolyte was then diluted so the concentration of the dominant cation (i.e., TiO^{2+}) was 0.1M. Supporting electrolyte background was separately collected and subtracted from the electrolyte spectra. To allow the comparison of cross-over values across experiments, an intensive, time independent measure, the permeation coefficient was used to describe the cross over rates. The permeation coefficient is defined as follows[64] –

$$P = \left(\frac{\ln\left(1-\left(\frac{2C_r}{C_0}\right)\right)\left(-\frac{Vl}{2A}\right)}{t} \right)$$

where C_r is the concentration measured at the receiving reservoir (determined using UV-Vis spectroscopy), C_0 is the active species concentration in the other electrolyte tank (0.5M or 0.9M), V is the volume of the receiving side (1 L), l is the membrane thickness (60-70 μm), A is the membrane area (25 cm2), and t is the time.

NMR characterization

All NMR measurements were carried out on a Bruker Avance 360 MHz NMR spectrometer. The ^{1}H-^{13}C heteronuclear multiple-quantum correlation spectroscopy (HMQC) measurements were carried out using gradient pulse for selection, incremental resolution of 1024 x 128 and 10 scans each. The samples for NMR spectra acquisition were prepared by dissolving approximately 50 mg of the polymer in 0.85 mL of deuterated dimethylsulfoxide. 35 mL of tetramethylsilane was added as an internal standard to all samples. The NMR spectra are presented in Supplementary Materials **Figs. S13-S15**.

Conclusions

A Ti-Ce ED-RFB was successfully developed for grid-scale energy storage applications for both diurnal load-leveling and LDES (multi-day to multi-week) use cases. This ED-RFB was enabled by a highly permselective AEM separator that exhibited < 0.4% cation crossover over 1000 hours of operation. The ED-RFB exhibited 100% capacity retention over 1300 hours diurnal cycling with >70% energy efficiency. Additionally, it exhibited close to 100% charge retention upon storage at 90% SOC for over 96 hours. Given this level of performance and capacity retention, the Ti-Ce ED-RFB promises to match and surpass the sub-decadal lifetime of Li-ion batteries. The Ti-Ce ED-RFB can be less expensive than DOE cost targets at both system cost and LCOS levels through multiple pathways (that can be deployed in parallel) such as **1)** improved power density, **2)** passive thermal management, **3)** operational automation and **4)** higher utilization rate (i.e., more cycles per year). In summary, the aqueous Ti-Ce ED-RFB incorporating earth-abundant elemental actives can be inexpensively deployed in frequency regulation and demand-response when coupled with an intermittent power source (such as solar or wind) while the modular nature and sub-linear cost scaling enable applications in weak grid and off-grid energy storage applications[1,2].

Declarations

Acknowledgements

The authors gratefully acknowledge financial support from the Advanced Research Projects Agency-Energy (ARPA-E), the US Department of Energy under award no. DE-AR0000768 as part of the Integration and Optimization of Novel Ion Conducting Solids (IONICS) program. The authors acknowledge with gratitude the McKelvey School of Engineering, Washington University in St. Louis and the Roma B. & Raymond H. Wittcoff Distinguished University Professorship. The authors thank the High-Resolution NMR Facility, Department of Chemistry at Washington University in St. Louis for access to facilities. The authors thank the Nano Research and Environmental Facility (NREF), a member of the National Nanotechnology Infrastructure Network (NNIN), which is supported by the National Science Foundation under Grant No. ECS-0335765 for access to facilities. The NREF is part of the McKelvey School of Engineering at Washington University in St. Louis.

Author contributions

S.S and V.R conceived the Ti-Ce ED-RFB. S.S identified electrolyte compositions, characterized them with the help of C.H and performed ED-RFB tests with the help of Y.Z. Y.Z prepared and characterized the separators used in this study. T.G prepared the cost models with input and help from S.S and V.R. All authors analyzed the data. S.S and V.R wrote the manuscript. All authors edited the manuscript. V.R supervised the project, obtained funding and instrumental facilities.

Competing interests

The authors currently have no financial interests that may be perceived to influence the conclusions presented in this work. The authors are seeking intellectual property protections on aspects of one or

more technologies described in this report through the Office of Technology and Management (OTM) at Washington University in St. Louis (WUSTL) and have filed US Patent Application 16/299,693 and PCT Patent Application WO2020028374A1.

Data Availability

All of the data associated with these studies are represented in the manuscript and supplemental information. The raw data are available from the corresponding author upon reasonable request.

Code Availability

This manuscript does not utilize custom codes or mathematical algorithms.

References

1. Dunn, B., Kamath, H. & Tarascon, J. for the Grid : A Battery of Choices. *Science (80-.).* **334**, 928 (2011).
2. Yang, Z. *et al.* Electrochemical Energy Storage for Green Grid. *Chem. Rev.* **111**, 3577–3613 (2011).
3. Obama, B. The irreversible momentum of clean energy. *Science (80-.).* **355**, 126–129 (2017).
4. Kittner, N., Lill, F. & Kammen, D. M. Energy storage deployment and innovation for the clean energy transition. *Nat. Energy* **2**, 1–6 (2017).
5. Department of Energy. Funding Opportunity Announcement Advanced Research Projects Agency – Energy (Arpa-E) Duration Addition to Electricity Storage (DAYS). *DE-FOA-0001906* (2017).
6. U.S Energy Information Administration. Levelized Cost and Levelized Avoided Cost of New Generation Resources in the Annual Energy Outlook 2018. *Annual Energy Outlook 2018* (2018). Available at: https://www.eia.gov/outlooks/aeo/pdf/electricity_generation.pdf.
7. Braff, W. A., Mueller, J. M. & Trancik, J. E. Value of storage technologies for wind and solar energy. *Nat. Clim. Chang.* **6**, 964–969 (2016).
8. Davies, D. M. *et al.* Combined economic and technological evaluation of battery energy storage for grid applications. *Nat. Energy* **4**, 42–50 (2019).
9. Nykvist, B. & Nilsson, M. Rapidly falling costs of battery packs for electric vehicles. *Nat. Clim. Chang.* **5**, 329–332 (2015).
10. Comello, S. & Reichelstein, S. The emergence of cost effective battery storage. *Nat. Commun.* **10**, 1–9 (2019).
11. Englberger, S., Jossen, A. & Hesse, H. Unlocking the Potential of Battery Storage with the Dynamic Stacking of Multiple Applications. *Cell Reports Phys. Sci.* 100238 (2020). doi:10.1016/j.xcrp.2020.100238
12. Abraham, K. M. Prospects and limits of energy storage in batteries. *J. Phys. Chem. Lett.* **6**, 830–844 (2015).

13. Soloveichik, G. L. Flow Batteries: Current Status and Trends. *Chem. Rev.* **115**, 11533–11558 (2015).
14. Dmello, R., Milshtein, J. D., Brushett, F. R. & Smith, K. C. Cost-driven materials selection criteria for redox flow battery electrolytes. *J. Power Sources* **330**, 261–272 (2016).
15. Darling, R. M., Gallagher, K. G., Kowalski, J. A., Ha, S. & Brushett, F. R. Pathways to low-cost electrochemical energy storage: a comparison of aqueous and nonaqueous flow batteries. *Energy Environ. Sci.* **7**, 3459–3477 (2014).
16. NASA. NASA redox storage system development project, calendar year 1982. *Nasa Tm-83469* **1**, (1983).
17. Fedkiw, P. S. & Watts, R. W. A mathematical model for the iron/chromium redox battery. *J. Electrochem. Soc.* **131**, 701–709 (1984).
18. Jalan, V., Morriseau, B. & Swette, L. Optimization and fabrication of porous carbon electrodes for Fe/Cr redox flow cells. *Nasa Cr-167921* (1982).
19. Gahn, R. F., Hagedorn, N. H. & Johnson, J. A. Cycling Performace of the Iron- Chromium Redox Energy Storage System Conservation and Renewable Energy. *Nasa Tm-87034* (1985).
20. Jalan, V., Stark, H. & Giner, J. Requirements for optimization of electrodes and electrolyte for the iron/chromium Redox flow cell. *Nasa Cr-165218* (1981).
21. Alexander, S. S. & Hodgdon, R. B. Anion permselective membrane. *Nasa Cr-135316* (1978).
22. Wesoff, E. Flow Battery Aspirant Imergy Has Let Go Its Staff and Is Selling Its Assets. *Green Tech Media* (2016). Available at: https://www.greentechmedia.com/articles/read/Flow-Battery-Aspirant-Imergy-Has-Let-Go-Its-Staff-and-Is-Selling-Its-Assets. (Accessed: 25th November 2020)
23. Rychcik, M. & Skyllas-Kazacos, M. Characteristics of a new all-vanadium redox flow battery. *J. Power Sources* **22**, 59–67 (1988).
24. Ulaganathan, M. *et al.* Recent Advancements in All-Vanadium Redox Flow Batteries. *Adv. Mater. Interfaces* **3**, 1–22 (2016).
25. Leung, P. K. *et al.* Characterization of a zinc-cerium flow battery. *J. Power Sources* **196**, 5174–5185 (2011).
26. Leung, P. K., Ponce De León, C. & Walsh, F. C. An undivided zinc-cerium redox flow battery operating at room temperature (295 K). *Electrochem. commun.* **13**, 770–773 (2011).
27. Leung, K. Two-electron reduction of ethylene carbonate: A quantum chemistry re-examination of mechanisms. *Chem. Phys. Lett.* **568–569**, 1–8 (2013).
28. Hawthorne, K. L., Wainright, J. S. & Savinell, R. F. Studies of Iron-Ligand Complexes for an All-Iron Flow Battery Application. *J. Electrochem. Soc.* **161**, A1662–A1671 (2014).
29. Gong, K. *et al.* All-Soluble All-Iron Aqueous Redox-Flow Battery. *ACS Energy Lett.* **1**, 89–93 (2016).
30. Na, Z., Xu, S., Yin, D. & Wang, L. A cerium–lead redox flow battery system employing supporting electrolyte of methanesulfonic acid. *J. Power Sources* **295**, 28–32 (2015).
31. Yun, S., Parrondo, J. & Ramani, V. A vanadium-cerium redox flow battery with an anion-exchange membrane separator. *Chempluschem* **80**, 412–421 (2015).

32. Wang, Z., Parrondo, J. & Ramani, V. Polystyrene-Block-Poly(ethylene-ran-butylene)-Block-Polystyrene Triblock Copolymer Separators for a Vanadium-Cerium Redox Flow Battery. *J. Electrochem. Soc.* **164**, 372–378 (2017).
33. Sankarasubramanian, S., Zhang, Y. & Ramani, V. Methanesulfonic acid-based electrode-decoupled vanadium–cerium redox flow battery exhibits significantly improved capacity and cycle life. *Sustain. Energy Fuels* (2019). doi:10.1039/C9SE00286C
34. Ulaganathan, M., Suresh, S., Mariyappan, K., Periasamy, P. & Pitchai, R. New Zinc-Vanadium (Zn-V) Hybrid Redox Flow Battery: High-Voltage and Energy-Efficient Advanced Energy Storage System. *ACS Sustain. Chem. Eng.* **7**, 6053–6060 (2019).
35. Luo, T. *et al.* Cr-Zn Redox Battery with NiFe 2 O 4 as Catalyst for Enhanced Degradation of Cr(VI) Pollution. *ACS Sustain. Chem. Eng.* **7**, 111–116 (2019).
36. Lin, K. *et al.* A redox-flow battery with an alloxazine-based organic electrolyte. *Nat. Energy* **1**, 16102 (2016).
37. Beh, E. S. *et al.* A Neutral pH Aqueous Organic–Organometallic Redox Flow Battery with Extremely High Capacity Retention. *ACS Energy Lett.* **2**, 639–644 (2017).
38. Yang, B. *et al.* High-Performance Aqueous Organic Flow Battery with Quinone-Based Redox Couples at Both Electrodes. *J. Electrochem. Soc.* **163**, A1442–A1449 (2016).
39. Milshtein, J. D., Su, L., Liou, C., Badel, A. F. & Brushett, F. R. Voltammetry study of quinoxaline in aqueous electrolytes. *Electrochim. Acta* **180**, 695–704 (2015).
40. Brushett, F. R., Vaughey, J. T. & Jansen, A. N. An all-organic non-aqueous lithium-ion redox flow battery. *Adv. Energy Mater.* **2**, 1390–1396 (2012).
41. Liu, Q. *et al.* Non-aqueous chromium acetylacetonate electrolyte for redox flow batteries. *Electrochem. commun.* **12**, 1634–1637 (2010).
42. Sleightholme, A. E. S. *et al.* Non-aqueous manganese acetylacetonate electrolyte for redox flow batteries. *J. Power Sources* **196**, 5742–5745 (2011).
43. Escalante-Garcia, I. L., Wainright, J. S., Thompson, L. T. & Savinell, R. F. Performance of a Non-Aqueous Vanadium Acetylacetonate Prototype Redox Flow Battery: Examination of Separators and Capacity Decay. *J. Electrochem. Soc.* **162**, A363–A372 (2014).
44. Hu, B. *et al.* Improved radical stability of viologen anolytes in aqueous organic redox flow batteries. *Chem. Commun.* **54**, 6871–6874 (2018).
45. Goulet, M.-A. & Aziz, M. J. Flow Battery Molecular Reactant Stability Determined by Symmetric Cell Cycling Methods. *J. Electrochem. Soc.* **165**, A1466–A1477 (2018).
46. Imabayashi, S. I., Kitamura, N., Tazuke, S. & Tokuda, K. The role of intramolecular association in the electrochemical reduction of viologen dimers and trimers. *J. Electroanal. Chem.* **243**, 143–160 (1988).
47. Beh, E. S. *et al.* A neutral pH aqueous organic- organometallic redox flow battery with extremely high capacity retention. *ACS Energy Lett.* **2**, 639–644 (2017).

48. Department of Energy. Funding Opportunity Announcement Advanced Research Projects Agency – Energy (Arpa-E) Integration and Optimization of Novel Ion Conducting Solids (IONICS). (2016).
49. Albertus, P., Manser, J. S. & Litzelman, S. Long-Duration Electricity Storage Applications, Economics, and Technologies. *Joule* **4**, 21–32 (2020).
50. Yun, S., Parrondo, J. & Ramani, V. Composite anion exchange membranes based on quaternized cardo-poly(etherketone) and quaternized inorganic fillers for vanadium redox flow battery applications. *Int. J. Hydrogen Energy* **41**, 10766–10775 (2016).
51. Yun, S., Parrondo, J. & Ramani, V. Derivatized cardo-polyetherketone anion exchange membranes for all-vanadium redox flow batteries. *J. Mater. Chem. A* **2**, 6605–6615 (2014).
52. Leung, P. *et al.* Progress in redox flow batteries, remaining challenges and their applications in energy storage. *RSC Adv.* **2**, 10125–10156 (2012).
53. Ke, X. *et al.* Rechargeable redox flow batteries: flow fields, stacks and design considerations. *Chem. Soc. Rev.* **47**, 8721–8743 (2018).
54. Yang, J. H., Yang, H. S., Ra, H. W., Shim, J. & Jeon, J. D. Effect of a surface active agent on performance of zinc/bromine redox flow batteries: Improvement in current efficiency and system stability. *J. Power Sources* **275**, 294–297 (2015).
55. Michael, F. Recent estimates of the abundances of the elements in the earth's crust. *Usgs* 1–6 (1953). doi:10.1134/S001670290601006X
56. Leung, P. K., Ponce De León, C., Low, C. T. J. & Walsh, F. C. Ce(III)/Ce(IV) in methanesulfonic acid as the positive half cell of a redox flow battery. *Electrochim. Acta* **56**, 2145–2153 (2011).
57. Kreh, R. P., Spotnitz, R. M. & Lundquist, J. T. Mediated Electrochemical Synthesis of Aromatic Aldehydes, Ketones, and Quinones Using Ceric Methanesulfonate. *J. Org. Chem.* **54**, 1526–1531 (1989).
58. Bard, A. J. & Faulkner, L. R. *Electrochemical Methods: Fundamentals and Applications*. *Electrochemical Methods: Fundamentals and Applications* (Wiley, 2000). doi:10.1016/B978-0-12-381373-2.00056-9
59. Li, Y., Parrondo, J., Sankarasubramanian, S. & Ramani, V. Impact of Surface Carbonyl- and Hydroxyl-Group Concentrations on Electrode Kinetics in an All-Vanadium Redox Flow Battery. *J. Phys. Chem. C* **123**, 6370–6378 (2019).
60. Nicholson, R. S. Theory and Application of Cyclic Voltammetry for Measurement of Electrode Reaction Kinetics. *Anal. Chem.* **37**, 1351–1355 (1965).
61. Sankarasubramanian, S., Kahky, J. & Ramani, V. Tuning anion solvation energetics enhances potassium–oxygen battery performance. *Proc. Natl. Acad. Sci. U. S. A.* **116**, 14899–14904 (2019).
62. Buchanan, C. A. *et al.* Structures and Free Energies of Cerium Ions in Acidic Electrolytes. *Inorg. Chem.* **59**, 12552–12563 (2020).
63. Klingler, R. J. & Kochi, J. K. Electron-transfer kinetics from cyclic voltammetry. Quantitative description of electrochemical reversibility. *J. Phys. Chem.* **85**, 1731–1741 (1981).

64. Xie, W. *et al.* Fundamental salt and water transport properties in directly copolymerized disulfonated poly(arylene ether sulfone) random copolymers. *Polymer (Guildf).* **52**, 2032–2043 (2011).
65. Arges, C. G. & Ramani, V. Two-dimensional NMR spectroscopy reveals cation-triggered backbone degradation in polysulfone-based anion exchange membranes. *Proc. Natl. Acad. Sci. U. S. A.* **110**, 2490–2495 (2013).
66. Zhang, Y., Parrondo, J., Sankarasubramanian, S. & Ramani, V. Detection of Reactive Oxygen Species in Anion Exchange Membrane Fuel Cells using In Situ Fluorescence Spectroscopy. *ChemSusChem* **10**, 3056–3062 (2017).
67. Sankarasubramanian, S., Zhang, Y. & Ramani, V. Methanesulfonic acid-based electrode-decoupled vanadium-cerium redox flow battery exhibits significantly improved capacity and cycle life. *Sustain. Energy Fuels* **3**, 2417–2425 (2019).
68. Gernon, M. D., Wu, M., Buszta, T. & Janney, P. Environmental benefits of methanesulfonic acid. *Green Chem.* **1**, 127–140 (1999).

Figures

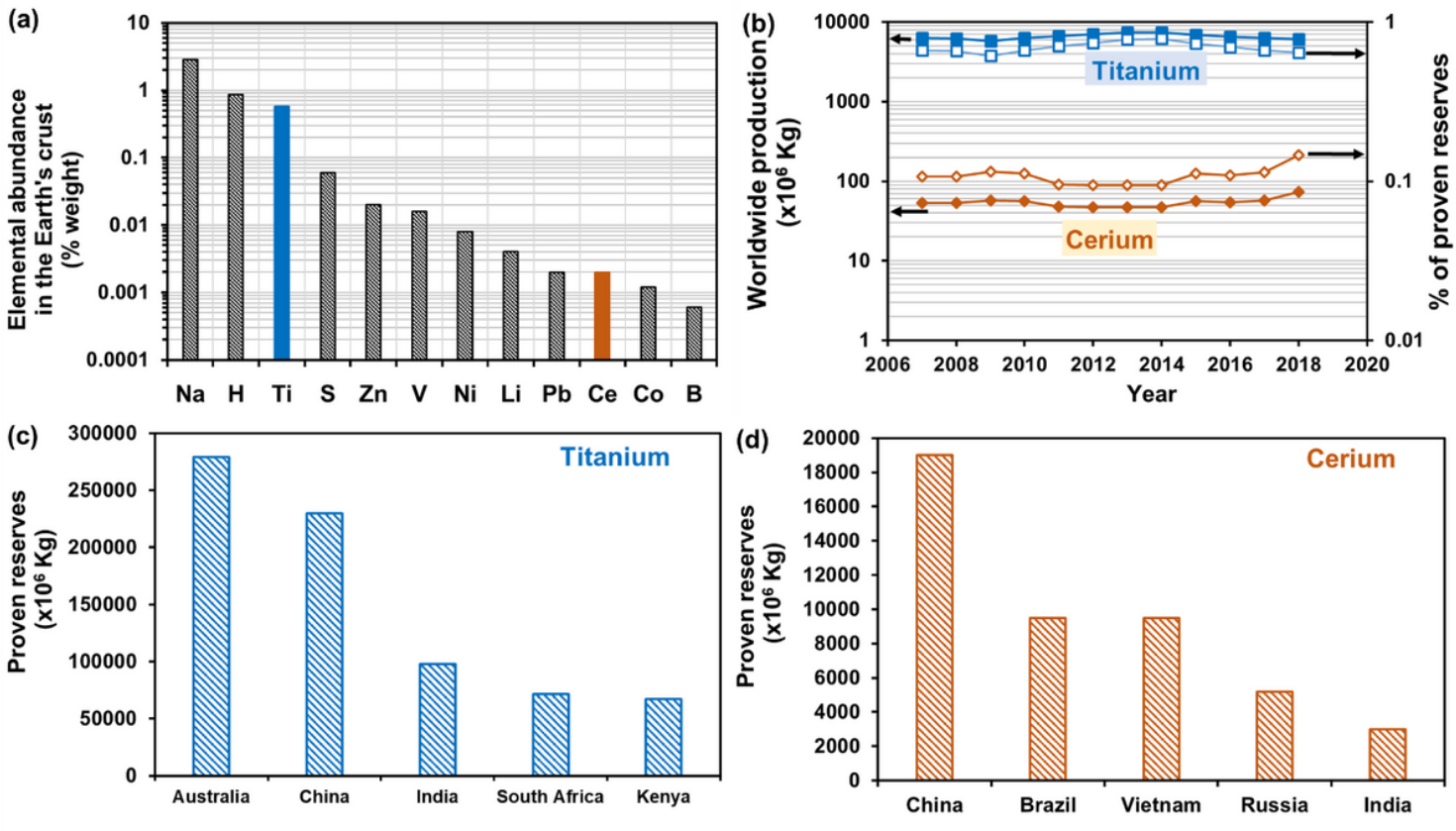

Figure 1

(a) Abundance of some common battery materials in the earth's crust; (b)Yearly production and corresponding rate of reserves exploitation for Ti and Ce over the past decade (c) Countries with top 5 proven reserves of Ti (d) Countries with top 5 proven reserves of Ce.

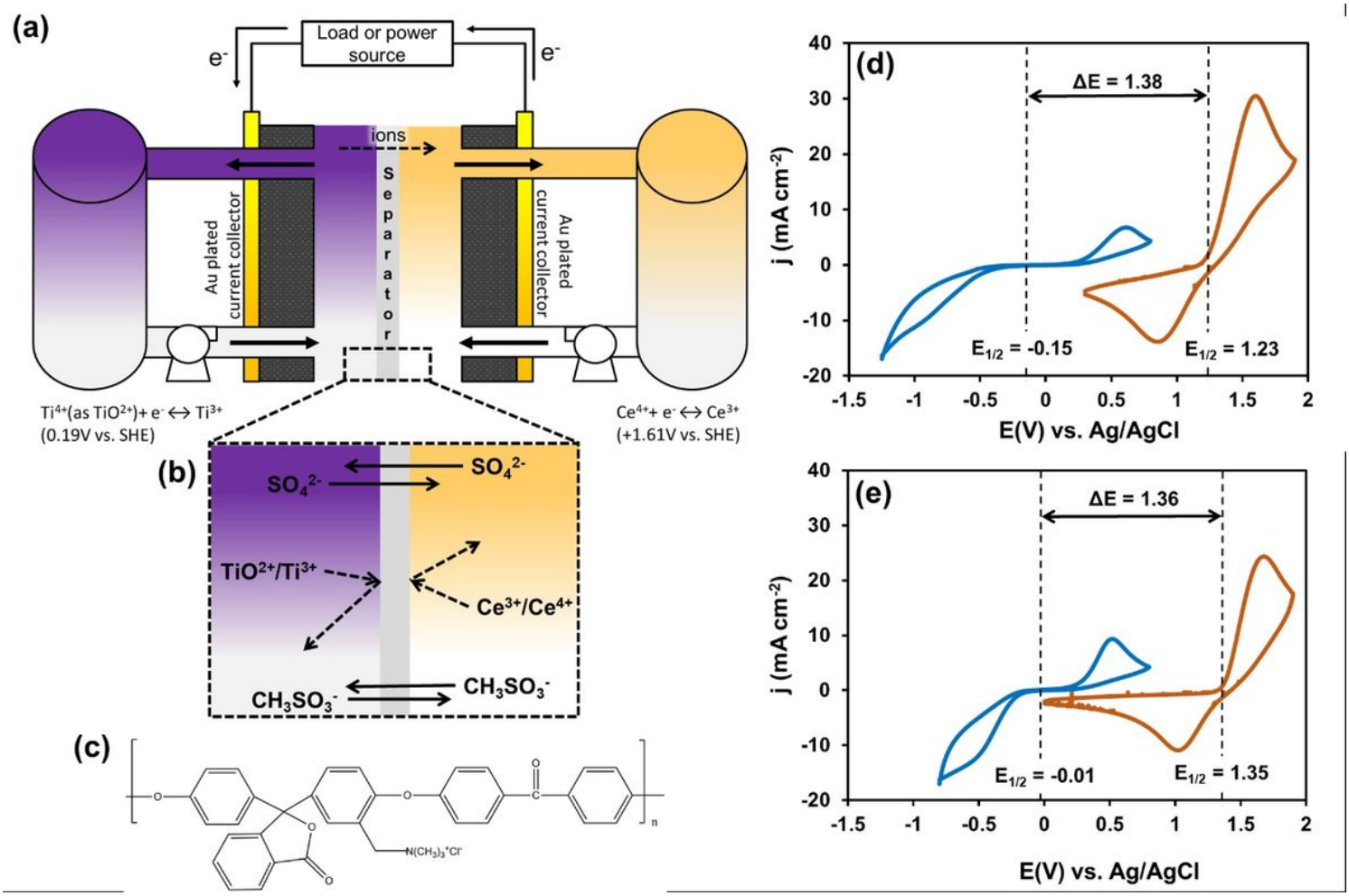

Figure 2

The Ti-Ce electrode-decoupled redox-flow battery (ED-RFB). (a) Schematic of the Ti-Ce ED-RFB, (b) ionic conduction through the anion exchange membrane (AEM) separator, (c) chemical structure of the quaternized cardo-poly(ether ketone) (QPEK-C) AEM separator, (d) cyclic voltammograms of the Ti and Ce active species in H2SO4 supporting electrolyte, (e) cyclic voltammograms of the Ti and Ce active species in CH3SO3H supporting electrolyte.

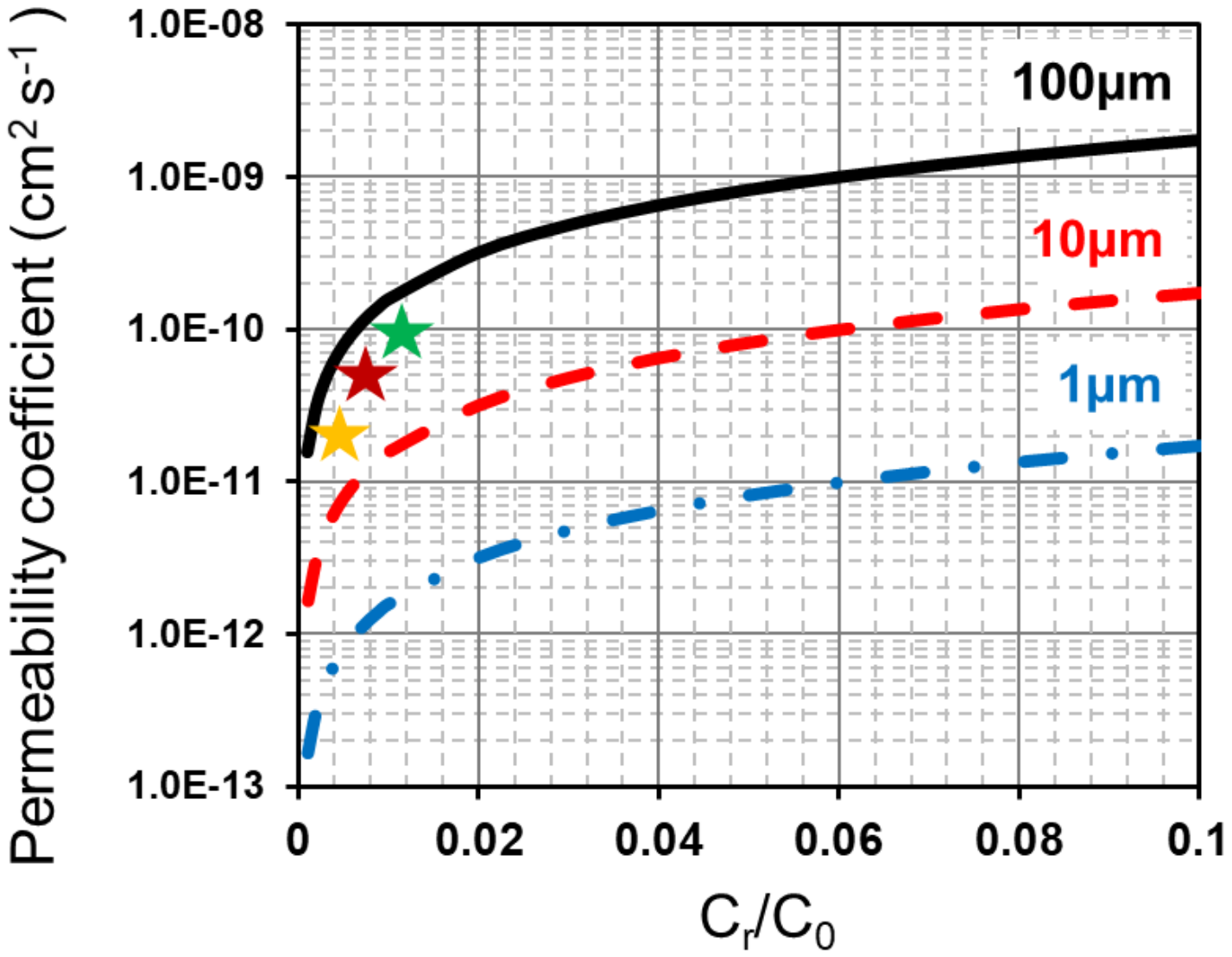

Figure 3

Redox active species permeability coefficient as a function of the ratio between species concentration in the receiving reservoir (Cr) to the species concentration in the source reservoir (C0). Permeability coefficient across separators of different thicknesses are provided as tie lines. The permeability coefficient across QPEK-C composite membranes with TiO2 (green star), SiO2 (red star) and Al2O3 (gold star) fillers is provided.

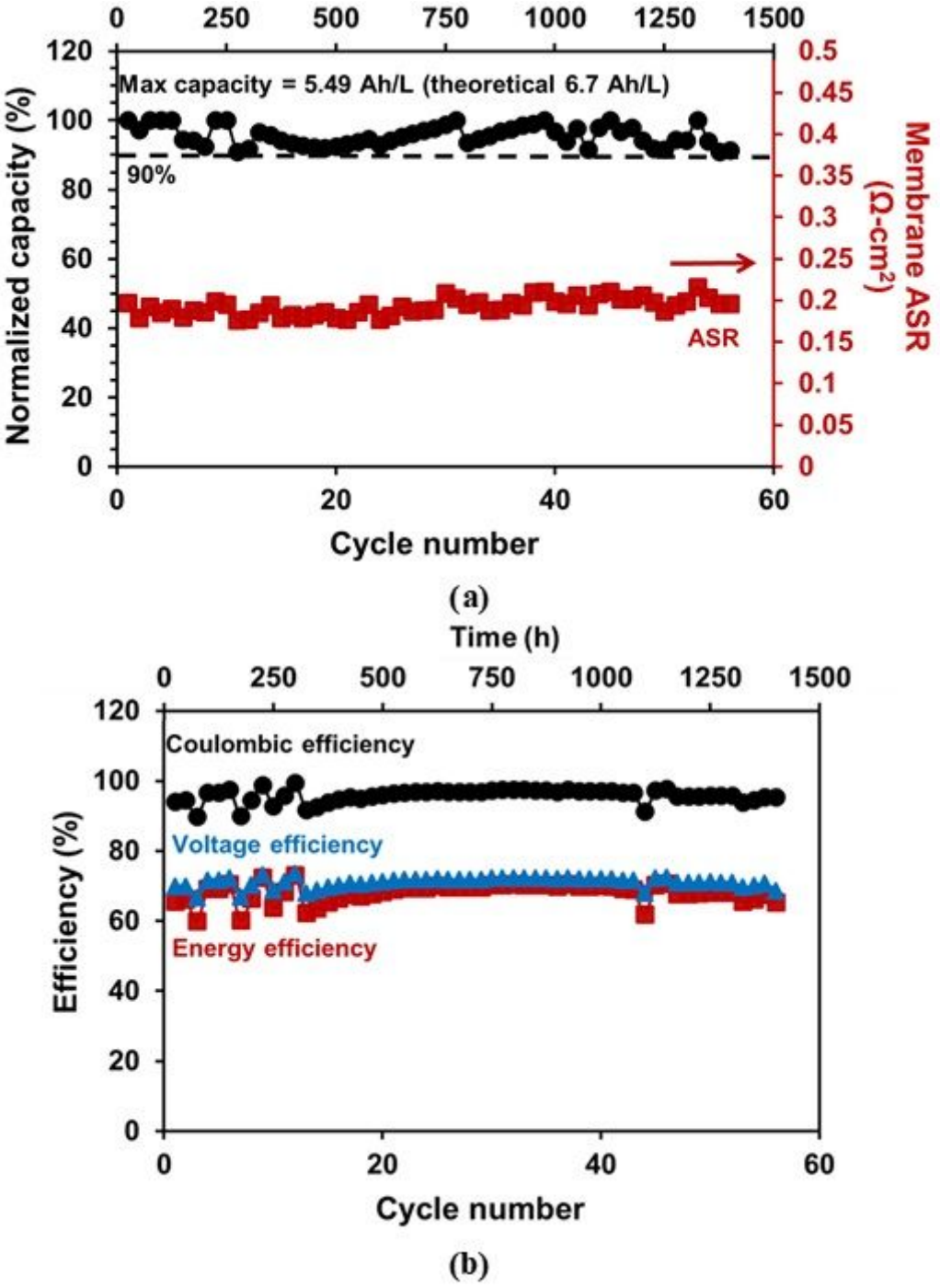

Figure 4

Performance of a H2SO4 based Ti-Ce ED-RFB with a QPEK-C-TMA + Al2O3 separator – (a) Normalized capacity and area specific resistance (ASR) over 1300 hours of cycling (56 cycles); (b) Coulombic, voltage and energy efficiencies corresponding to each cycle in panel (a). Additional cycling data is presented in the Supplementary Materials.

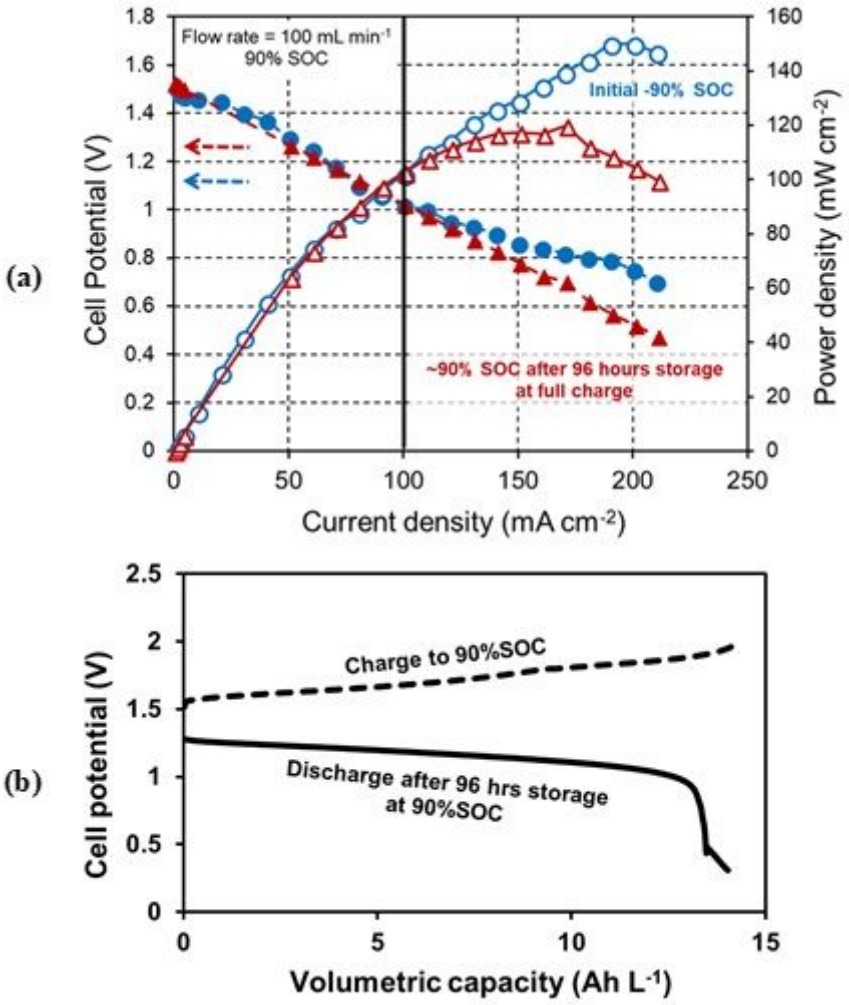

Figure 5

Performance of a CH3SO3H based Ti-Ce ED-RFB - (a) Polarization curves before and after extended storage (96 hours) at 90% SOC following long-duration cycling of the Ti-Ce ED-RFB (cycling data shown in Supplementary Materials) (b) Charge-store-discharge curve corresponding to the half cycles before and after storage at 90% SOC. Additional cycling data is presented in the Supplementary Materials.

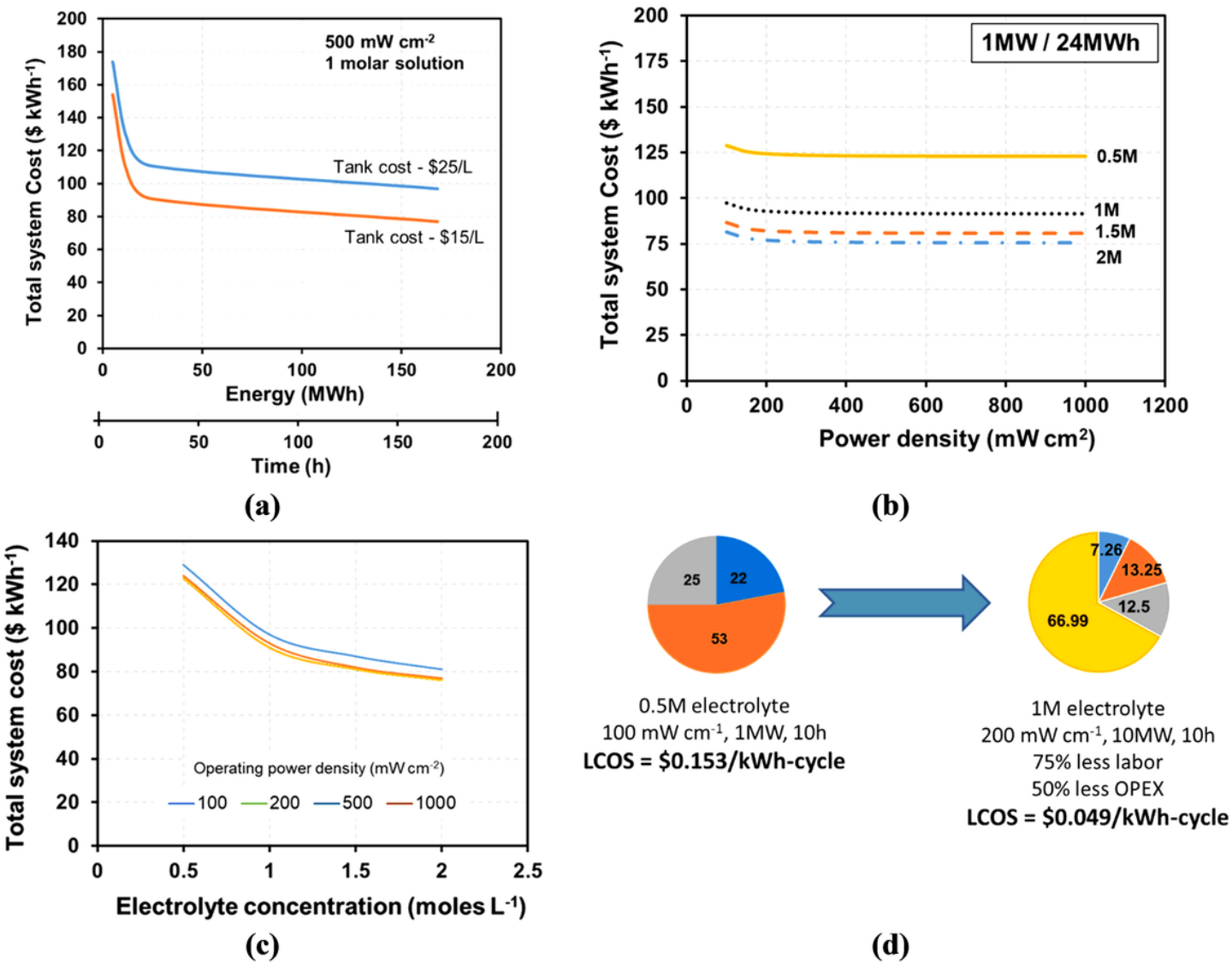

Figure 6

Economics of the Ti-Ce ED-RFB Impact of (a) cycle duration; (b) power density; (c) electrolyte concentration on system installed cost and (d) one (of many) pathway to achieving LCOS<$0.05/KWh-cycle. All calculations depicted are for the H2SO4 based system. Economics of the CH3SO3H based system and pathways to LCOS as low as $0.025/kWh-cycle can be found in the Supplementary Materials.

Supplementary Files

This is a list of supplementary files associated with this preprint. Click to download.

- ESITiCe121120.docx